

Article

# An efficient optimized deep learning model for diabetic retinopathy classification

Mary Vespa Mathiazhagan<sup>1,\*</sup>, Agees Kumar Chellappan<sup>2</sup><sup>1</sup> Department of Computer Science and Engineering, Vel Tech Rangarajan Dr. Sagunthala R&D Institute of Science and Technology, Chennai 600062, Tamilnadu, India<sup>2</sup> Department of Electrical and Electronics Engineering, Arunachala College of Engineering for Women, Vellichanthalai 629203, Tamilnadu, India\* **Corresponding author:** Mary Vespa Mathiazhagan, [vespace@gmail.com](mailto:vespace@gmail.com)

## CITATION

Mathiazhagan MV, Chellappan AK. An efficient optimized deep learning model for diabetic retinopathy classification. *Journal of Biological Regulators and Homeostatic Agents*. 2025; 39(2): 3293. <https://doi.org/10.54517/jbrha3293>

## ARTICLE INFO

Received: 10 February 2025

Accepted: 4 March 2025

Available online: 25 March 2025

## COPYRIGHT



Copyright © 2025 by author(s).

*Journal of Biological Regulators and Homeostatic Agents* is published by Asia Pacific Academy of Science Pte. Ltd. This work is licensed under the Creative Commons Attribution (CC BY) license.

<https://creativecommons.org/licenses/by/4.0/>

**Abstract:** One of the most common disorders worldwide is diabetes, a metabolic condition marked by elevated blood sugar levels. Complications from diabetes can lead to diabetic retinopathy (DR). Later stages of DR can result in blindness, while early stages may only produce slight vision abnormalities or no symptoms at all. Diagnosing diabetic retina (DR) is particularly challenging due to changes in the retina that occur with the stages of the illness. An autonomous DR early detection device can help ophthalmologists with DR screening while also protecting a patient's vision. The Ensemble of EfficientNet-B0, a unique approach based on the Modified Sparrow Search Algorithm (EMSSA) that provides more accurate classification with less processing time, is presented in this study. The proposed EMSSA regularized classification is carried out after the images have been pre-processed, segmented, and dimension-reduced features constructed using the suggested algorithms. Five phases of non-proliferative images were used in the experiment: Proliferative, moderate, mild, severe, and non-proliferative. By using dimensionally reduced data, the suggested approach reduces complexity and produces an accuracy rate of 98.8%. According to an examination of performance metrics, the system performs better than other cutting-edge methods in terms of F-measures, accuracy, recall, and precision.

**Keywords:** diabetic retinopathy; Image Net; blindness; EfficientNet-B0; deep learning

## 1. Introduction

Diabetes-related retinopathy, or DR, is one of the leading causes of vision impairment. The diabetic patient's retinal veins are severed by the DR [1]. Apart from denoting the initial phases of the illness, the word "NPDR" is additionally separated into three classifications: mild, moderate, and severe. A miniature aneurysm (MA) is a little, spherical red dab near the end of a vein [2]. As the MAs tear into deeper layers, the retina experiences a flame-shaped hemorrhage in the moderate stage [3]. In each of the four quadrants, there are around twenty intraregional hemorrhages in the severe stage. Moreover, there are obvious intraregional microvascular abnormalities and significant venous hemorrhage. PDR is the high-level phase of DR that causes revascularization, which is the unconstrained development of fresh blood vessels on the surface of the retina through working microvascular organizations [4].

By 2025, there will be 592 million DR victims around the world, up from 382 million at present [5]. As per a review [6] carried out in the Pakistani region of Khyber Pakhtunkhwa (KPK), 30% of diabetic patients had DR, with 5.6% of them dying blindly as a result. If the mild NPDR is not treated in its early phases, it eventually turns into PDR. 130 patients with DR symptoms were observed in Sindh, Pakistan,

according to another survey [7]. An estimated 25.8% of all patients evaluated had a PDR diagnosis, which accounted for 23.85% of all out-DR patients [8].

Patients with DR are asymptomatic in the early stages, but as the condition progresses, floaters, distortions, blurred vision, and a progressive loss of visual acuity develop [9]. Subsequently, to forestall the serious impacts of later stages, it is essential, however hard, to perceive the DR in the beginning phases [10]. The diagnosis of DR is made using color fundus pictures, as was previously mentioned [11]. Because only highly skilled domain experts are able to perform manual analysis, it is costly both in terms of time and money [12]. In order to help doctors and radiologists, it is crucial to automatically analyze fundus images using computer vision techniques [13]. The two categories of computer vision-based techniques are end-to-end learning [14] and involved designing [15]. The standard procedures utilized by the active designing strategies to remove highlights—like Hoard, Filter, LBP, Gabor channels, etc.—neglect to encode the distinctions in scale, turn, and brightening. Start-to-finish inclining improves classification performance by automatically learning the hidden rich features [16,17]. The DR in Kaggle dataset 1 is recognized utilizing an assortment of manual designing and end-to-end learning-based procedures [18–20], but no strategy can distinguish the mild stage. Early control of this dangerous illness relies upon the recognizable proof of the mild stage. The objective of this work is to utilize start-to-finish profound gathering organizations to recognize all phases of medication obstruction. The outcomes demonstrate that the suggested strategy works better than cutting-edge techniques.

DL-based techniques, as described by Sebastian et al. [21], are frequently chosen for creating DR detection systems. This was accomplished through a review of the literature on the use of deep learning for diagnosing diabetic retinopathy based on fundus images and a brief overview of the methods that researchers are currently employing to investigate this problem. According to Uppamma et al. [22], the study's distinctive contributions include the following: first, giving a thorough history of the DR illness and the conventional methods of detection. Second, a presentation is given of the many deep learning applications and imaging techniques in DR. Third, the many real-world situations and use cases related to deep learning algorithms for DR detection are examined.

Mohanty and associates [23] For DR identification and order, recommend two profound learning (DL) designs: DenseNet 121 is a half-breed network that combines the XGBoost Classifier and VGG16. The two DL models were evaluated using preprocessed retinal images from the APTOS 2019 Visual Deficiency Discovery Kaggle Dataset. In this review, Fayyaz et al. [24] utilized a deep learning network with AlexNet and ResNet101-based highlight extraction to consequently perceive and classify DR fundus pictures in light of seriousness. Ant Colony systems frameworks additionally help with choosing the highlights, and interconnected layers help in distinguishing the significant qualities or properties.

The new approach by Venkaiahppalaswamy et al. [25] combines a deep learning method with a strong crossover binocular Siamese to classify the DR image. To start with, to take out undesired clamors, a pre-processing stage is laid out. It is focused on utilizing the cross-directed bilateral filter (CGBF) technique to carry out this. The study's objective, according to Gao et al. [26], is to create a multilevel classification

deep learning model for FFA pictures that may be used clinically and includes lesion categorization and pre-diagnosis assessment. Agarwal et al.'s study [27] thoroughly examines a number of recently proposed frameworks for classifying exudates, hemorrhages, microaneurysms, and non-proliferative diabetic retinopathy that depend on AI and deep learning organizations. Specialists have utilized various promising pre-prepared deep learning models to sort various phases of medication revelation. They have additionally investigated moving picking up utilizing pre-prepared models like GoogLeNet, AlexNet, VGG, and so on [28]. It has been noted that nearly all of the freely accessible public and private data sets for study are unbalanced. Generative adversarial organizations (GANs) and their variations were additionally utilized to create name-safeguarding information to relieve these issues.

### **Problem statement**

Image processing is utilized in the medical field to accurately diagnose illnesses. To increase DR detection's automation, applicability, and accuracy, advancements over earlier methods are required. They also make working with big training data sets necessary, which adds complexity to the system. Certain automated classification methods have the potential to classify data erroneously or take longer to classify. It is crucial to decrease processing time while increasing the accuracy of picture categorization on large datasets. Based on the Modified Sparrow Search Algorithm (EMSSA) approach, they thereby present a completely new EfficientNet-B0. This approach produces a regularized grouping result and limits the framework's applicability to low-dimensional data.

The paper's primary contribution is as follows:

- The DR images' quality is enhanced by using modified histogram equalization as a preprocessing to boost the performance rate.
- The Sparse Subspace can be utilized to effortlessly identify the DR pictures for division. The working environment is recognized using the clustering approach. From the DR image, segmentation precisely extracts the region of the eye associated with a lesion.
- To create a PCA-integrated texture feature-based classification system and identify the subset of texture properties that will improve classification accuracy.
- To create an automated system for classifying different grades of DR images, an Ensemble of EfficientNet-B0 based on the Modified Sparrow Search Calculation (EMSSA) calculation is likewise suggested as a classifier. It likewise lessens the intricacy of the design to regularize the classification yields.

The increasing prevalence of diabetic retinopathy (DR) underscores the urgent need for more efficient and accurate early detection methods. The proposed EMSSA approach addresses this gap by enhancing classification accuracy while reducing computational complexity, ultimately aiding in timely diagnosis and vision preservation.

There are multiple sections in this document. The following document's Section 2 provides an explanation of the recommended system's architecture. Section 3 describes the experimental results and observations. The suggested task is concluded in Section 4.

## 2. Proposed methodology

The use of potent machine learning approaches, such as deep learning, has successfully completed clinical imaging tasks such object recognition, segmentation, and classification. While typical CNNs rely on feature extraction techniques, DL algorithms may be able to use the information immediately.

Consequently, deep learning methods have been applied in a variety of fields, including bioinformatics, finance, clinical imaging, pharmaceutical development, and education. The suggested system uses an Ensemble of EfficientNet-B0 based on the Modified Sparrow Search Algorithm (EMSSA) to provide an end-to-end method for DR classification. **Figure 1** depicts the planned DR layout block outline.

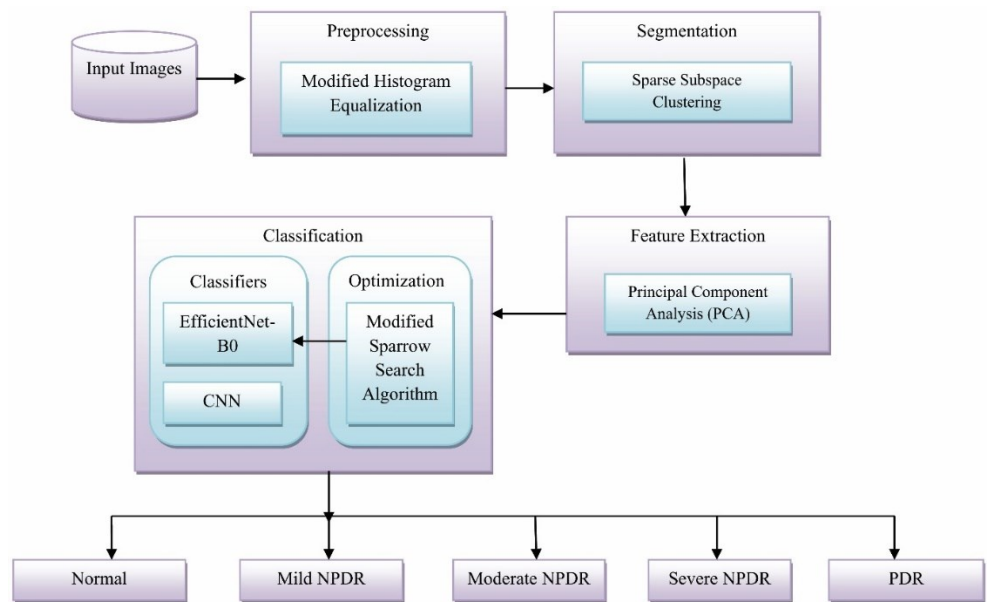


**Figure 1.** Block schematic for the suggested structure.

### 2.1. Dataset

There are 850 images of the fundus in the dataset, ranging in resolution from 385 mild to 780 moderate, 194 severe, and 296 proliferating. Make training and testing sets with 361 and 550 pictures, separately, from the 435-image dataset. The sample input photos are shown in **Figure 2**. The Image Net dataset has been used to identify the following levels of diabetic retinopathy (DR): Proliferative, mild, moderate non-proliferative, severe non-proliferative, normal, and ordinary.

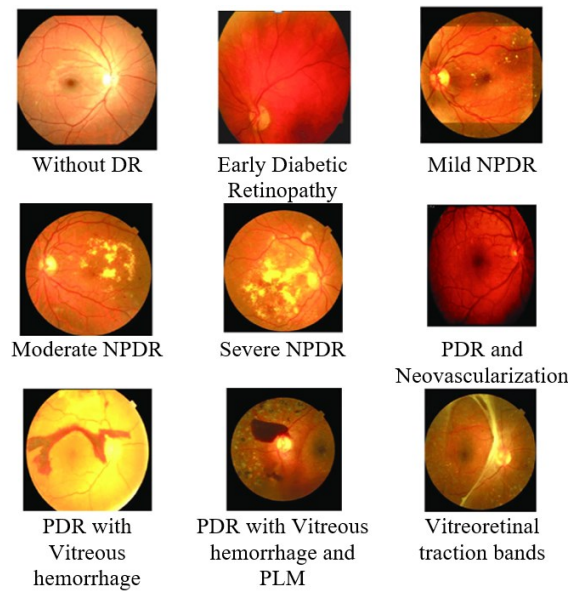


**Figure 2.** Sample images.

## 2.2. Preprocessing

The process of preparing fundus photographs enhances their quality and eliminates extraneous noise. Some features of an image can be enhanced through preprocessing. A number of factors come into play, including noise reduction, processing time, cost, and image quality at input. Image pre-processing is applied. It is possible to apply a linear method algorithm to any pixel without specifying whether or not the image is contaminated. Only pixels can be processed using nonlinear algorithms in order to ascertain whether or not they are contaminated. After that, damaged photos were eliminated by applying a specific algorithm.

### Modified histogram equalization

Histogram balance is a strategy that can be utilized to change the power levels of photos to support contrast. Then, the result district's histogram is contrasted with the other one that was given. To build the difference of the fundus picture seen in **Figure 3**, histogram equalization is applied. To do this, the histogram is adjusted. The histogram only indicates the frequency at which every one of the dark levels, which range from 0 to 255, happens. The fundus picture is created utilizing the different upgrade approach.

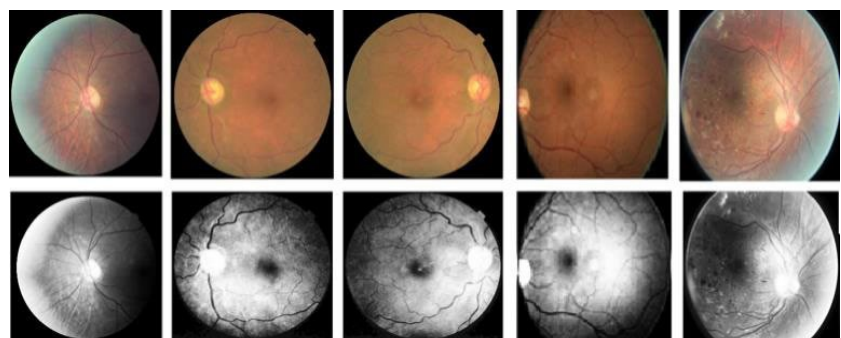


**Figure 3.** Database of fundus images for histogram equalization.

This is an advancement over the traditional modified histogram equalization method. When compared to traditional histogram equalization, the quantitative and qualitative assessments of modified histogram equalization would help elucidate how the changed technique enhances feature extraction, contrast preservation, or noise reduction. It is evident that every bar on the equalized histogram has the same height based on the histogram's physical interpretation. That is what it is, that is,

$$p_s(s)ds = p_r(r)dr \quad (1)$$

Assume that  $s = T(r)$  is a monotonically growing function, and that  $r = T^{-1}(s)$  is the interval in which it exists. Based on Equation (1), we can infer:

$$p_s(s) = \left[ p_r(r) \frac{1}{ds/dr} \right]_{r=T^{-1}(s)} = p_r(r) \frac{1}{p_r(r)} = 1 \quad (2)$$

Relationship mapping for the conventional graph equation algorithm: Connection between  $f_i$ , the grey value of the pixels in the upgraded picture under various circumstances, and  $I$ , the grey color of the pixels in the first picture.

$$f_i = (m - 1)T(r) = (m - 1) \sum_{k=0}^i \frac{q_k}{Q} \quad (3)$$

In the first image, the total amount of grey levels visible is denoted by  $[Q]_k m$ , where  $Q$  is the number of pixels through the  $k$ -th dim level and is the total amount of pixels throughout the image. The entropy of the  $i$ -th conceal is  $p_i$  on the off chance that an image has  $n$  various shades of dim and the probability that the  $i$ -th shade will emerge is

$$p_i \times e(i) = -p_i \log p_i \quad (4)$$

The overall image's entropy is

$$E = \sum_{i=0}^{n-1} e(i) = - \sum_{i=0}^{n-1} p_i \log p_i \quad (5)$$

The approach was developed using the following equation:

$$Output_{hist} = \frac{Input_{hist} - Min_{hist}}{Max_{hist} - Min_{hist}} \quad (6)$$

The output picture for image contrast enhancement is denoted by  $Output_{hist}$ , and the original image's histogram values with its minimum and maximum range are represented by  $Max_{hist}$  and  $Min_{hist}$ .

### 2.3. Segmentation

Picture segmentation is the method involved with separating a picture into non-overlapping sections; one sort of picture segmentation is subspace portrayal. The coefficient requires scanty information to be placed in the clustering matrix of similitude results. The block outline of sparse subspace clustering is displayed in **Figure 4**.

A process called sparse subspace clustering is used to group elements of the same class into subspaces and extract ROI from them. Computational and Numerical Techniques in Medication. An image contains many objective pictures with convoluted structures, yet its elements comprise low-dimensional subspace

information. Eventually, the sparse subspace clustering approach has been used to perform segmentation. The processing item in this pixel-level fusion method is a pixel. Multimodal diabetic retinopathy tissue information is extracted from multimodal DR pictures and combined into a single modal DR image using the linear fusion approach. Therefore, multimodal image segmentation is simplified by reducing it to single-modal picture segmentation. The activity of direct combination is as per the following.

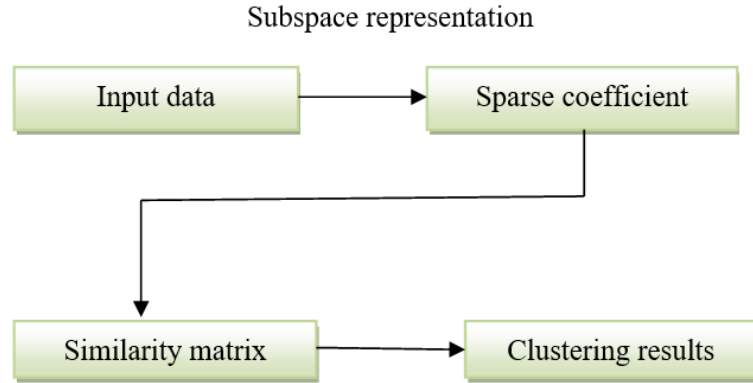


**Figure 4.** Block diagram of sparse subspace clustering.

$$F_{ij} = \alpha T_1(i, j) + \beta T_2(i, j) + \varepsilon T_3(i, j) \quad (7)$$

Here,  $F_{ij}$  represents the fused picture;  $T_1(i, j)$ ,  $T_2(i, j)$ , and  $T_3(i, j)$  address the pixel upsides of  $T_1$ ,  $T_2$ , and  $T_3$  at position  $(i, j)$ ; and  $\alpha$ ,  $\beta$ , and  $\varepsilon$  signify the loads of every modular picture. Applying the direct combination process,  $\alpha + \beta + \varepsilon = 1$ ,  $T_1:T_2:T_3 = 3:2:1:4$ . The SSC-based multimodal picture segmentation calculation comprises the accompanying advances:

- The combined picture will be separated into  $N$  super pixel blocks utilizing input  $I$  utilizing the preprocessing method.
- Super pixel blocks yield  $D$ -dimensional feature vectors that are extracted into an element grid  $\{X_i\}$  ( $i = 1, 2, \dots, n$ ).
- Get the framework  $C$  of sparse coefficients.
- The similarity matrix  $W = |C| + |C^T|$  is calculated, with  $W_{ij} = W_{ij} = |C_{ij}| + |C_{ij}|$
- The outcome of the clustering procedure is acquired.

## 2.4. Feature extraction

Large amounts of unstructured data are broken up and compressed into smaller, more manageable collections by a process called feature extraction, which is part of the dimensionality reduction process. In the end, the handling complexity dropped to a manageable level. The Method of Feature Extraction Since there are many factors in the real world of these massive data sets, Principal Component Analysis (PCA) is the most important component. PCA is one statistically based feature extraction technique. This is the fundamental PCA formula.

$$R\varphi_j = \lambda_j\varphi_j(j = 1, 2, \dots) \quad (8)$$

Let us assume that an  $n$ -dimensional input sample  $x$  has a form.

$$y = A^T x \quad (9)$$

$Y$  is found to be  $M$ -dimensional. If  $Y$  is an extracted feature of  $X$ , meaning that it contains most of the information linked to  $X$ 's extracted features, then obtaining this transformation matrix  $A$  is the first stage in the feature extraction process using the PCA method. Equation (10) indicates that since  $A$  is made up of  $m$ -number eigenvectors,  $A$  might meet the requirements for the sources. The problem is then transformed into an eigenvector selection problem, where the smallest square error of  $Y$  and  $x$  is found in matrix  $A$ , which contains the elements generated by Equation (10). The estimated value of  $x$  is:

$$x = \sum_{j=1}^m \alpha_j \varphi_j + \sum_{j=m+1}^n b_j \varphi_j \quad (10)$$

The discrepancy between  $x$  and the retrieved values is

$$x = x - x = \sum_{j=m+1}^n (\alpha_j - b_j) \varphi_j \quad (11)$$

Mean square error is

$$\varepsilon^2 = E[\|x\|^2] = \sum_{j=m+1}^n [(\alpha_j - b_j)^2] \quad (12)$$

Equation (13) clearly shows that when the mean square error falls, it should fulfill

$$b_j = E[\alpha_j] \quad (13)$$

According to the equation, the constant should be replaced with the anticipated value of the remaining 13. When it is further converted, that is, when a new coordinate system is made using the overall mean as the origin, Equation (14) is solved.

$$b_j = E[\alpha_j] = E[\varphi_j^T x] = \varphi_j^T E[x] = 0 \quad (14)$$

$$\varepsilon^2 = \sum_{j=m+1}^n E[\alpha_j^2] = \sum_{j=m+1}^n E[(\varphi_j^T x)(\varphi_j^T x)^T] = \sum_{j=m+1}^n E[(\varphi_j^T x x^T \varphi_j)] = \sum_{j=m+1}^n \varphi_j^T R \varphi_j = \sum_{j=m+1}^n \lambda_j \quad (15)$$

These are the corresponding autocorrelation matrix  $R$  and eigenvector for the  $x$  Eigen values. The mean square error falls as Equation (16) shows. As a result, post-feature extraction, the energy retention rate is defined if it meets the subsequent formula.

$$\frac{\sum_{j=1}^m \lambda_j}{\sum_{j=0}^{n-1} \lambda_j} \quad (16)$$

The following are the steps to extract the entire PCA feature:

- The mean vector of the mode population serves as the coordinate system's origin.
- The autocorrelation matrix  $R$  is obtained.
- The autocorrelation matrix's  $R$  Eigen values are obtained.
- Sorting is carried out using the obtained Eigen values. The Eigen vectors are then calculated.

## 2.5. Classification technique (EMSSA)

Classifiers are algorithms that, after the decreased highlights from the brain area have been recovered, are used to classify pictures into their separate regions.

### 2.5.1. Efficient Net-B0 Model

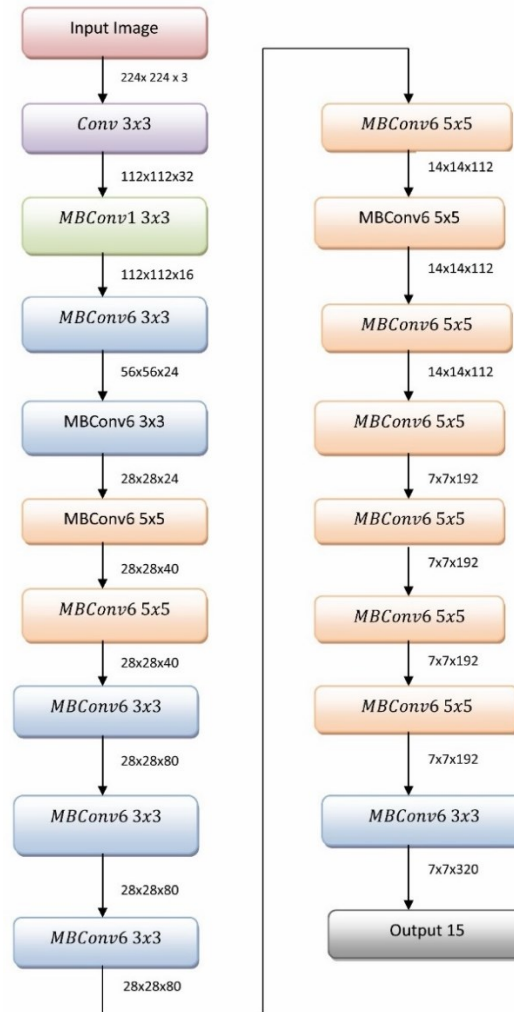


**Figure 5.** EfficientNet-B0 architecture.

The pre-processed picture at the top was made explicitly to be the contribution for this model. It is important to upgrade the CNN model in light of imperfections like Disappearing Slope. The Google Brain Group presented the Efficient Net Model in 2019. Mobile Net served as the foundation for Efficient Net. Mobile Net was established to develop a deep learning model. In Mobile Net, both point and depth scaling are applied. On the other hand, the fundamental model Efficient Net B0 is based upon the squeeze and excitation blocks, as well as the reversed bottleneck remaining blocks MobileNetV2. The schematic portrayal of the EfficientNet-B0 design is shown in **Figure 5**.

Furthermore, the Efficient Net model is said to include about 20 layers. The development of the Efficient Net model involved adjusting network depth, width, and resolution, as well as intently analyzing model adaptability. To adjust the versatility of depth, width, and resolution, the Productive Net worldview was referenced. Amplifying model precision inside the given limitations is one of the different targets of the Effective Net model.

The Effective Net gauge model depends on convolutional layer obstructs and reversed lingering blocks (MbConv), the two of which were used in the MobileNetV2 model prior. The actuation layer and group standardization layer would be situated after the convolution layer in the Convolutional Layer Block. Notwithstanding these layers, this powerful net model likewise incorporates an excitation block and a press block. The main goal of the Efficient Net model’s squeeze and excitation blocks is to significantly improve the model’s functionality.

**2.5.2. Modified sparrow search algorithm**

Taking into account the fundamental details, sparrows are gregarious creatures that belong to the bird family and live and breed in groups. They have extremely quick flights. The majority of sparrows have lovely, melodic vocals.

The two components of the sparrow’s food-searching mechanism are producers and screeners. Producers seek to accommodate a food supply, while scroppers depend on producers to meet their energy requirements. More food-producing sparrows face off against scavengers. Due to their meager energy stores, sparrows are more susceptible to attack. The discovery of this type of food in sparrows led scientists to create a novel metaheuristic called the Sparrow Search Algorithm. Typically, the SSA begins with a random individual matrix that indicates where the sparrows are located as follows:

$$X = [x_{1,1} \cdots x_{1,d} \cdots x_{n,1} \cdots x_{n,d}] \tag{17}$$

where  $d$  is the developed parameters dimension and  $n$  is the number of sparrows.

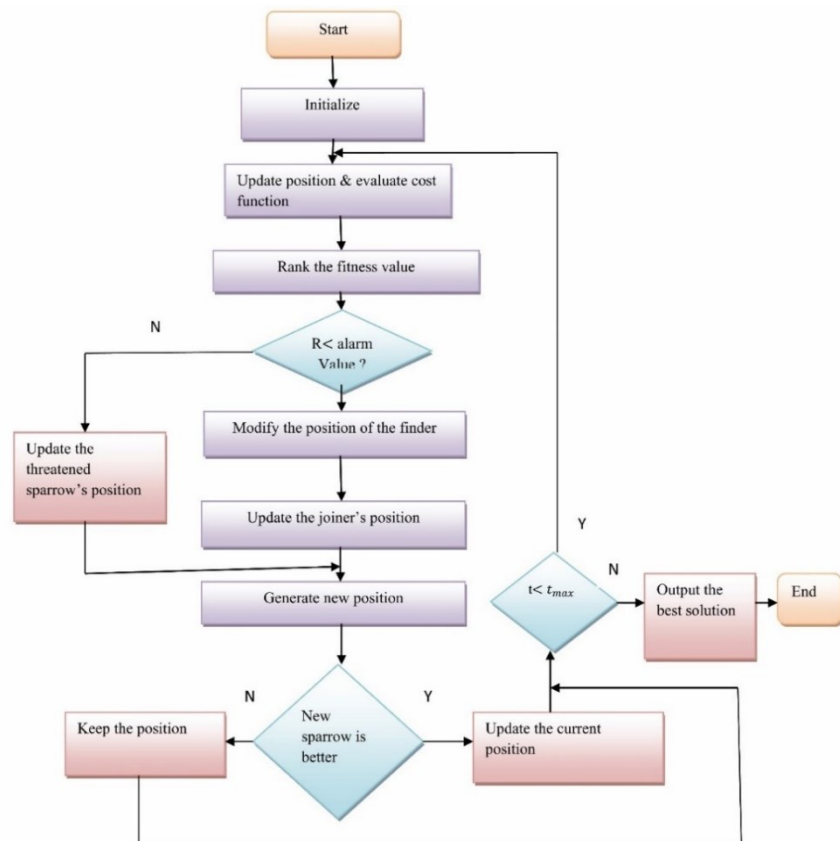


**Figure 6.** Flowchart of modified sparrow search algorithm.

By determining their costs, the cumulative energy collections have been completed. The formula below is used to compute individual costs.

$$F_x = [f([x_{1,1}, x_{1,2}, \dots, x_{1,d}])f([x_{2,1}, x_{2,2}, \dots, x_{2,d}]) \dots f([x_{n,1}, x_{n,2}, \dots, x_{n,d}])] \quad (18)$$

**Figure 6** displays a flowchart of the modified Sparrow Search Algorithm. The problem of producers searching throughout a wide range of the solution space for food sources is expressed mathematically as above.

$$X_{i,j}^t = \{X_{i,j}^t \times \exp\left(-\frac{i}{b \times t_{max}}\right) X_{i,j}^t + Q \times \text{Lif} R_2 \geq T_s \text{if } R_2 < T_s \quad (19)$$

$$j=1, 2, 3, \dots, d$$

where  $b$  is an irregular number somewhere in the range of 0 and 1, and  $X_{i,j}^t$  is how much the  $j$ -th aspect of the  $i$ -th person is at iteration  $t$ . The variables  $t$ ,  $L$ ,  $Q$ , and  $R_2$  represent the current iteration, the  $d$ -dimension vector, the normally distributed random integer, and the concerning quantity in the interval  $[0,1]$ .  $T_s$ : Safety threshold inside the interval  $[0.5, 1]$ .

This can be expressed mathematically as follows:

$$X_{i,j}^{t+1} = \{Q \times \exp\left(\frac{x_{worst}^t - x_p^{t+1}}{i^2}\right) \text{if } i > \frac{n}{2} X_p^{t+1} + |X_{i,j}^t - X_p^{t+1}| \times A^\dagger \times L \quad (20)$$

$$A^\dagger = A^T \times (A \times A^T)^{-1} \quad (21)$$

where  $A$  is a vector that is randomly distributed between  $X_{worst}$  and  $X_p$ , which stand for the producer's ideal position and the current global worst position, respectively. The stance for sparrows that understand the danger is as follows.

$$X_{i,j}^{t+1} = \{X_{best}^t + \alpha \times |X_{i,j}^t - X_{best}^{t+1}| \text{if } f_i > f_g |X_{i,j}^t + K \times \left(\frac{|X_{i,j}^t - X_{worst}^{t+1}|}{(f_i - f_w) + \varepsilon}\right) f_i = f_g \quad (22)$$

where  $f_i$  is the ongoing person's expense,  $f_g$  and  $f_w$  are the ongoing worldwide ideal and most pessimistic scenario wellness sums, individually;  $\varepsilon$  is a value near zero to zero for forestalling zero-division error;  $\alpha$  is a haphazardly dispersed esteem with a fluctuation of 1 and an average measure of 0; and  $K$  is a random value in the range. Furthermore,  $X$  best represents the current global optimal situation.

$$\hat{x}_{n,d} = -x + \underline{x} - x_{n,d} \quad (23)$$

Thus, given a genuine vector  $x_{n,d} \in \mathbb{R}^n$ , the opposing direction is determined by  $-x \leq x_{n,d} \leq x$  and  $x_{n,d} \in \mathbb{R}^n$ .

The best candidate is then chosen depending on how well they can carry out the necessary function, and the opposed value is compared to the genuine value. Another change is to make use of the Merit function (MF).

$$x_{i+1,d} = \left\{ \frac{m(x_{i-1,d})}{m(x_{i-1,d})} x_{i,d}, m(x_{i,d}) \geq m(x_{i-1,d}) x_{i,d}, m(x_{i,d}) < m(x_{i-1,d}) \right. \quad (24)$$

where the following equation yields  $m(x_{i-1,d}) \geq 0$ , which explains the MF.

$$m(X^i) = \|X^i - \frac{\nabla^\dagger g(X^i) X^i}{\nabla^\dagger g(X^i) \nabla g(X^i)} \nabla g(X^i)\|^2 + \frac{g(X^i)^2}{g(X^0)^2} \quad (25)$$

The above indicates that  $x_{i+1,d} < x_{i,d}$ . By suitably changing the network's weights, a novel modified version of the Sparrow Search Algorithm (MSSA) replaces back propagation in CNN in order to minimize Mean Square Error (MSE), which is the difference between the planned and output values. The proposed EMSSA model's training algorithm is given below in Algorithm 1.

---

**Algorithm 1** The proposed EMSSA model's training algorithm

---

- 1: Input: Baseclassifierlist: EMSSAclassifier\_list, Trainingset: dataset: data\_valid,
  - 2: Validationset: data\_train
  - 3: Testset: data\_test.
  - 4: Output: Base classifier EMSSA value: F1\_list; test set sample's initial prediction probability value: Test\_pro.
  - 5: Establish the test set sample's beginning probability value list.
  - 6:  $M = 0$ .
  - 7: do for  $j = 1$  to  $K$
  - 8: do for  $i = 1$  to  $N$
  - 9: as opposed to  $M < Iteration$
  - 10: Take the player out of the basic classifier and load the weight
  - 11: "imageNet," then obtain the model: basis\_model.
  - 12: Place the categorization model's output layers module after *base\_model*.
  - 13: The training set, *data\_train\_process*, and the validation set  
 $M = M + 1$ ;
  - 14: end while
  - 15: end for
  - 16: Using  $m$  as the sample number for the test set, the test determined the category  $Tm$  of the final test sample by choosing the category with the highest probability value.
- 

### 3. Experimental result

The MATLAB code for the proposed setup was created on a Windows computer with a CPU speed of 4.6 GHz and 4 GB of RAM. By constructing an information base query, the sample image may be found. The model's confusion matrix, recall, accuracy, precision, and F1-score were all evaluated. Accuracy bends were also developed to filter the model's display according to the number of ages. The dataset used to assess if the suggested method was appropriate was Image Net. The Image Net collection contains ten high DR microscopic photographs. There are 845 photos available. A little less than half of the photographs were utilized in preparing, and 80% were utilized in testing. These photographs are delivered by preprocessing, which raises the difference and nature of the picture.

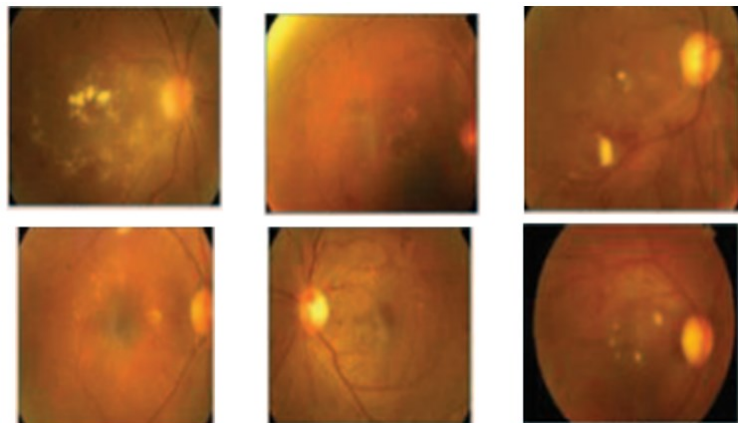


**Figure 7.** Sample of input images from Image Net dataset.

EMSSA is recommended as a way to improve classification performance because **Figure 7** shows that the information test pictures from the Image Net dataset are inadequate for precise characterization. The example pictures go through preprocessing strategies to diminish commotion and further develop picture quality. These are the final features that were taken from the example photos. Ultimately, the classification process is used to determine the levels of severity and improve accuracy.

A Windows machine with a CPU speed of 4.6 GHz and 4 GB of RAM was used to write the MATLAB code for the suggested setup. The information base is questioned to track down the picture of the example. We inspected the exactness, accuracy, precision, F1-score, and confusion matrix of the review's model. Exactness bends were also created to track how the model fared in relation to the number of epochs.

An inquiry into the data set is done in order to locate the sample image. The F1-score, accuracy, precision, recall, and confusion matrix of the reviewed model were examined. Additionally, precise bends were created to check the number of ages in the model's presentation. The Picture Net dataset is utilized to evaluate the efficacy of the suggested process. Ten small images with significant DR are included in the Image Net dataset. 845 images are available. Approximately 40% of the photos were utilized for testing, while the remaining 80% were used for processing. To create these images, preprocessing is used, which enhances the image's quality and uniqueness.

The Image Net dataset is utilized to evaluate the suitability of the proposed approach. Ten high DR minute photographs are remembered for the Image Net dataset. There are 845 pictures accessible. A little less than half of the photographs were utilized in preparing, and 80% were utilized in testing. These photographs are created by preprocessing, which raises the differentiation and nature of the picture. **Figure 7** represents that the information test pictures from the picture Net dataset are inadequate for exact order; subsequently, EMSSA is proposed for the purpose of improving grouping execution. EMSSA is prescribed as a method for further developing grouping execution since **Figure 7** shows that the information test pictures from the picture Net dataset are lacking for exact order. Following the application of preprocessing techniques to reduce noise and improve image quality, the following features were ultimately recovered from the sample images: Ultimately, the classifying process is utilized to determine the severity levels and improve accuracy.

### **3.1. Preprocessing**

In the suggested method, modified histogram equalizations are utilized for the pre-processing of DR pictures. As seen in **Figure 8**, the filter sharpens and smooths the image's edges. When pre-handling techniques are used prior to the completion of further division, the pixel quality of the image is enhanced. Preprocessing is an essential stage in any classification process since it prepares an image for further processing. The RGB image is typically converted to grayscale for study purposes.

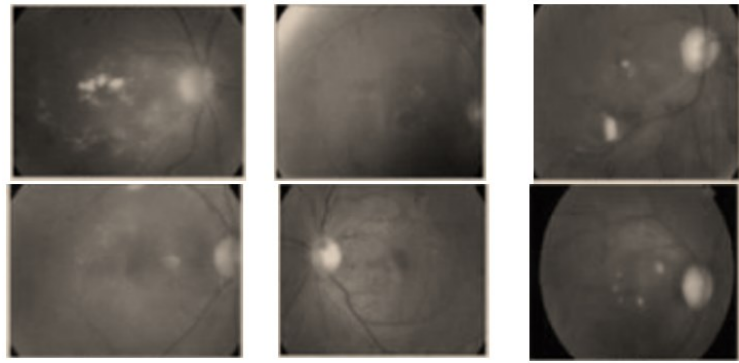


**Figure 8.** Pre-processed image.

### 3.2. Segmentation

After preprocessing, the acquired image is put into the segmentation algorithm, which separates the DR images. The segmented image is displayed in **Figure 9**; segmentation is carried out using sparse subspace clustering. Here, the optic disc, blood vessel, and microaneurysms are divided. The technique of optical disc detection tends to extend the boundaries of foreground bright spots in an image, much like the dilation process. Segmentation based on related components for the purpose of detection.

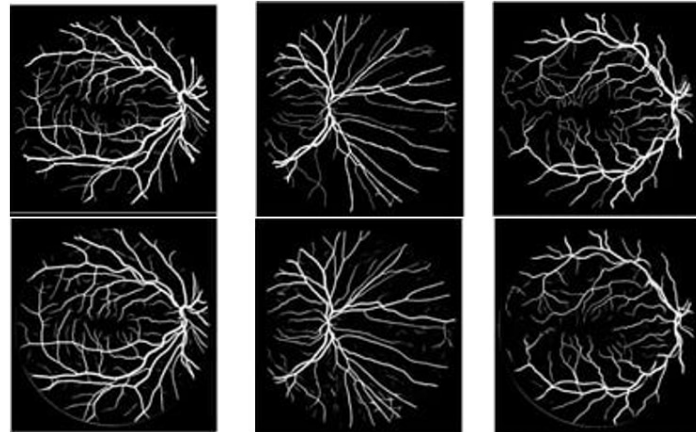


**Figure 9.** Segmented image.

### 3.3. Classification

The EMSSA classifier uses PCA techniques to lower the portioned highlights, and then separates the retinal images into normal, mild, moderate non-proliferative, serious non-proliferative, and proliferative classes. The proposed approach altogether outflanks existing strategies for beginning phase DR determination. The boundaries utilized in the plan of the proposed model are recorded in **Table 1**.

**Table 1.** The value of the proposed model's hyperparameters.

Hyper parameter	Value
Loss-function	Cross-category entropy
Number of Epochs	80
Quantity of batches	20

**Table 1.** (Continued).

Hyper parameter	Value
rate of dropouts	0.9
Rate of learning	0.005
Method of Tuning	Scheduler for Learning Rates
Convolutional layers	17, 22, 35 with size $6 \times 6$
The maximum pooling layer	$3 \times 3$
The Fully connected layers	700 and 200 units

Events that are appropriately ordered are handled by the components of the large diagonal elements, as shown in **Figure 10**. When an issue involves many classes, the number of lines and segments in the dataset’s disorder lattice is equal to the number of different classes in the dataset. The disarray network is used to create the perceptions of TP, TN, FP, and FN for every class. A variety of execution parameters, such as F1 score, review, accuracy, and exactness, are surveyed while taking the perceptions into account. **Table 2** provides the F1-score, recall, accuracy, and precision for each of the five classes. **Table 2** shows the proportion of moderate and non-serious DR cases that the model anticipated for every DR grade. Despite being assigned non-serious DR cases, some safe NPDR patients are considered excessive. To determine the F1 score, review and accuracy estimations are utilized. **Figure 11** shows an examination of the outcomes for every one of the five classes. The viability of the model was evaluated utilizing the F1-score, the weighted normal for recall and precision, and the proposed order technique.

	Normal	Mild NPDR	Moderate NPDR	Severe NPDR	PDR
Normal	99	0	1	0	0
Mild NPDR	1	98	0	1	0
Moderate NPDR	0	1	99	0	0
Severe NPDR	0	0	0	99	1
PDR	0	0	1	0	99

**Figure 10.** Confusion matrix.

**Table 2.** Performance indicators derived from the confusion matrix observations and expressed as a percentage.

	Accuracy	Precision	Recall	Specificity	F1-score
Normal	97.4	97	99	98.2	97
Mild DR	96.8	99	98	97.8	98.3
Moderate DR	98	97	98	98.2	97.44
Severe DR	99.5	98.5	96	96.7	98.64
PDR	99.2	97.6	97	99.5	98

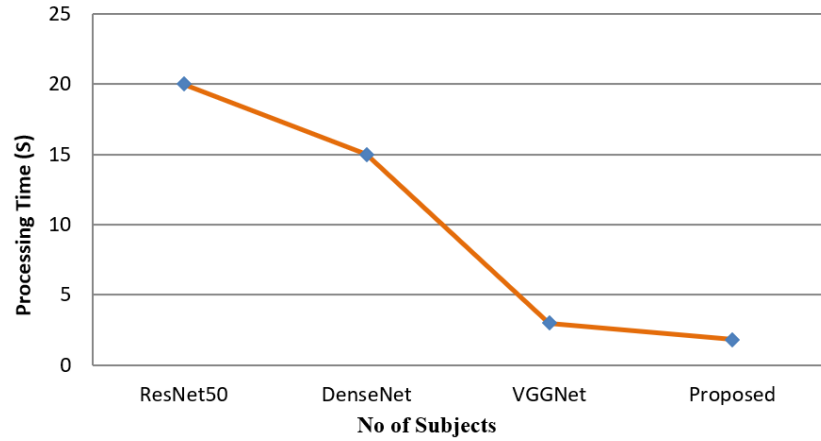


**Figure 11.** The suggested segmentation’s computation time.

### 3.4. Performance metrics

The percentage of samples that were successfully and wrongly identified is displayed by the confusion matrix values. False Positive (FP), False Negative (FN), True Positive (TP), and True Negative (TN) respect classes make up the chaos grid. The identified injuries are subject to the execution requirements for accuracy, responsiveness, and identification. True positive (TP): The test would be positive if there was a growth input.

True negative (TN): If the input had nothing to do with the tumor, the test would be negative.

False positive (FP): The result is favorable when the input is not a tumor.

False negative (FN): Should there be a tumor input, the result would be adverse.

Sensitivity or Recall:

To evaluate the capacity to accurately detect DR lesions, the following standards are applied:

$$Sensitivity = \frac{TP}{TP+FN} \quad (26)$$

Specificity:

The specificity, which is represented as, can be used to measure how well DR lesions can be ruled out.

$$Specificity = \frac{TN}{TP+FP} \quad (27)$$

Accuracy:

Using the formula, the lesion detection performance is determined.

$$Accuracy = \frac{TP+TN}{TP+TN+FP+FN} \quad (28)$$

Precision:

An ML model’s precision gauges how well it can forecast positive cases. It demonstrates how the full set of true positive evaluations and the false positive gauges that are real positives are related.

$$Precision = \frac{TP}{(TP+FP)} \quad (29)$$

F1-score:

To describe the F1-s, the symphonious approaches for accuracy and recall are applied. To process the F1-score, the following equation is used:

$$F1 - Measure = (2 \times P \times R)/(P + R) \quad (30)$$

False-positive rate (FPR):

The percentage of all negative test results that still yield positive results.

$$FPR = \frac{f}{f} + b \quad (31)$$

False-negative rate (FNR):

The proportion of positive test results that nevertheless yield negative results.

$$FNR = e/e + a \quad (32)$$

A balanced error rate (BER)

It is a humble blunder rate that records for both positive and negative outcomes.

$$BER = 1 - 0.5 \times ((sensitivity + specificity)/100) \quad (33)$$

$$NPV = g/g + d$$

where,  $g$  and  $d$  stand for the deceptive positive and false negative features, as well as the real positive and true negative traits, separately.

### 3.5. Performance analysis

In order to assess their individual performances, this section contrasts the pre-processing strategy, suggested segmentation calculation, proposed dimensionality decrease calculation, suggested regularization, and the successful EfficientNet-B0 with MSSA classification with other approaches that are currently in use.

#### 3.5.1. Segmentation analysis

Dice coefficient. The correctness of the segmentation findings is examined using the Dice coefficient. The segmentation accuracy obtained using different techniques is displayed in **Table 3**. It is shown that the Dice Coefficient value of 0.975 of the suggested work is much higher than that of earlier approaches.

**Table 3.** Segmentation evaluation.

Methods	Dice Coefficient
ResNet50	0.685
DenseNet	0.794
VGGNet	0.789
Proposed	0.978

Additionally, **Table 4** below provides details on the testing data segmentation period. We evaluate the suggested method's computing efficiency against four other approaches. The proposed process and the division techniques proposed by other authors are analyzed and totaled. Semantic segmentation for the proposed framework takes 1.80 s, which is far quicker than different frameworks showed.

**Table 4.** Comparative evaluation of various methods' segmentation times.

Methods	Processing Time
ResNet50	20 s
DenseNet	15 s
VGGNet	2–3 s
Proposed	1.80 s

Computation time also referred to as running time is the period of time expected to complete a calculation. The suggested segmentation algorithm is contrasted with the current techniques in **Figure 11**.

**Table 5** shows the preparation limits used to copy the suggested framework. The comparison between the recommended dropout regularization process and the usual technique is displayed in **Table 6**. With the recommended approach, a reduced deficit of 0.398, training accuracy of 0.917, and test accuracy of 0.9289 were achieved. These results were likewise attained by our suggested strategy.

**Table 5.** Training specifications.

<b>No of Epochs</b>	<b>50</b>
Quantity in Batch	20
Rate of Dropouts	0.5
Rate of Learning	0.001

**Table 6.** Performance comparison of the proposed dropout regularization method and the conventional method.

Parameters	Conventional dropout	Proposed dropout
Accuracy of Training	0.855	0.917
Loss of Training	0.458	0.398
Test Precision	0.846	0.929

### 3.5.2. Classification analysis

BER and NPV. **Table 7** presents a comparison of the suggested system's BER and NPV utilizing other approaches, such as ResNet50, DenseNet, and VGGNet. It shows that the recommended strategy yielded greater BER (0.015) and NPV (0.985) rates when compared to alternative approaches.

**Table 7.** NPV and BER comparison.

Parameters	BER	NPV
Proposed	0.015	0.985
ResNet50	0.07	0.70
DenseNet	0.13	0.8
VGGNet	0.16	0.55

Sensitivity and specificity. A comparison of the suggested method's sensitivity and specificity with other approaches is shown in **Figure 12**. It displays the

performance of the recommended system compared to a number of methods, such as ResNet50, DenseNet, and VGGNet. We compare the proposed strategy with alternative methods in terms of specificity and sensitivity performance. The recommended method yielded greater rates than other approaches in terms of specificity (98%) and sensitivity (97.5%).

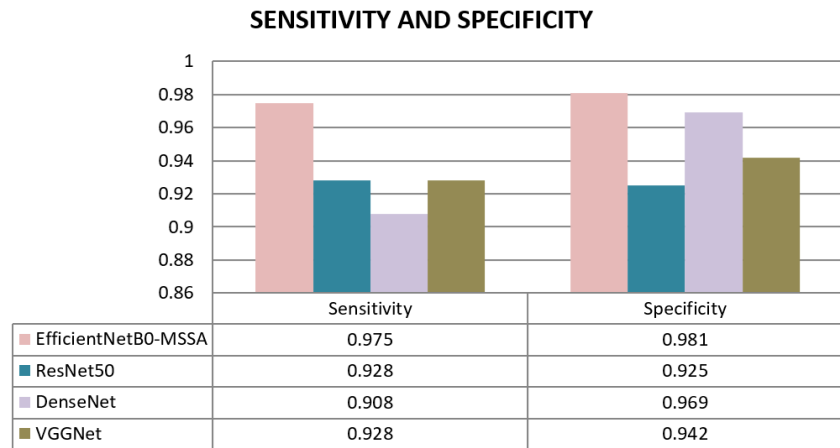


**Figure 12.** Sensitivity and specificity diagram.

Precision and F-measure. **Figure 13** compares the proposed framework with other techniques, including ResNet50, DenseNet, and VGGNet, in terms of precision and F-measure. The discoveries showed that the suggested methodology performed better compared to different techniques as far as F-measure (97.8%) and precision (98.8%).

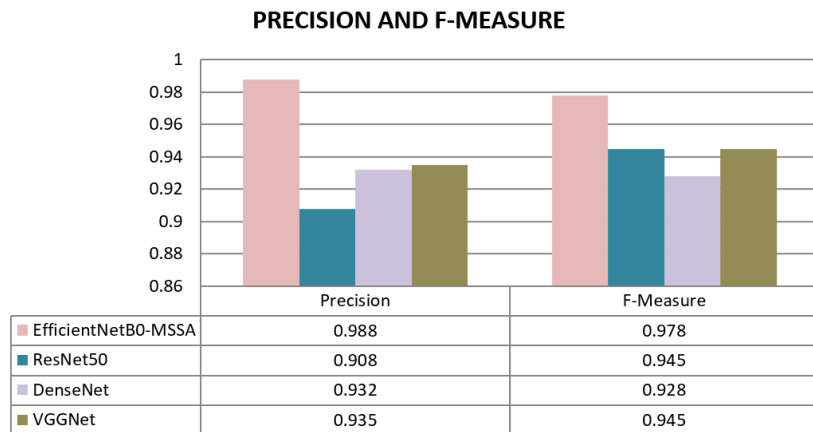


**Figure 13.** Precision and F-measure comparison.

FPR and FNR. The accuracy and F-measure analysis of the proposed framework using several methods, including ResNet50, DenseNet, and VGGNet, are displayed in **Figure 14**. The discoveries showed that the suggested technique performed better compared to different strategies as far as F-measure (97.8%) when compared to alternative alternatives.

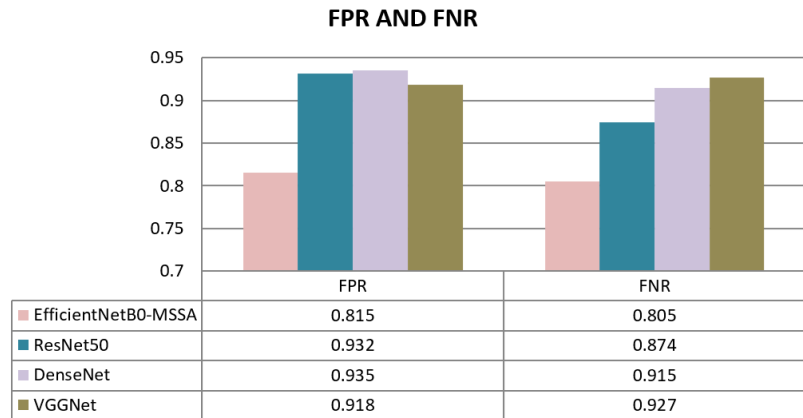


**Figure 14.** FPR and FNR comparison.

Accuracy vs. Epoch. The accuracy versus epoch graph that was acquired during the approval and preparation stage is shown in **Figure 15**. It delineates how significant the recommended framework is.

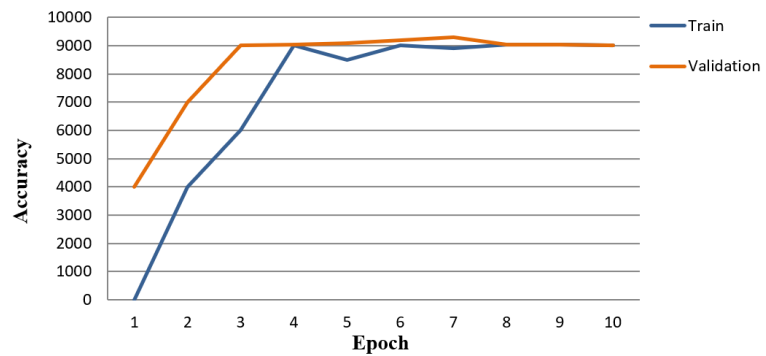


**Figure 15.** Accuracy vs. Epoch graph.

ROC curves. **Figure 16** displays the region under the ROC curve (AUC), a useful metric for evaluating a device’s ability to distinguish between two diagnostic characterizations. the ROC curves that various deep learning algorithms generate. When compared to other approaches, the proposed EMSSA strategy exhibits a larger location (Ac) under the ROC curve, indicating that it is closer to 1. Thus, the proposed approach has the best discriminating power.

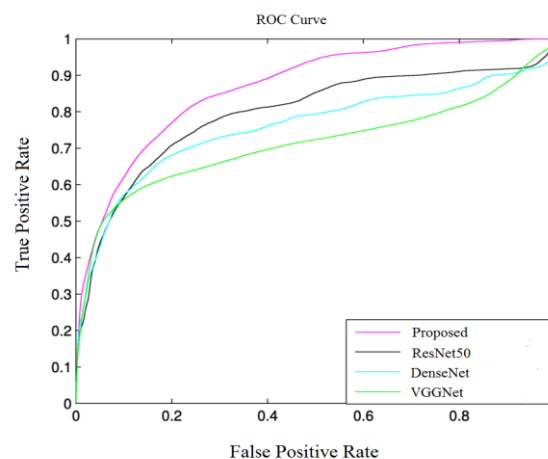


**Figure 16.** ROC curve.

Analyzing the accuracy of several different state techniques in comparison. **Table 8** presents a comparison between the accuracy of a state-of-the-art strategy and the suggested solution employing various systems. It demonstrates that the suggested strategy offers a 98.8% accuracy rate, which is more noteworthy than other cutting-edge techniques. Compared to other cutting-edge techniques, the suggested EMSSA employed to categorize the brain images produces superior results.

**Table 8.** The suggested method's performance is compared to that of several other existing algorithms.

Method	Accuracy	Recall	Specificity	Sensitivity	Precision	F-Measure
AlexNet	87	77.9	82.2	78.8	82	95.24
NN-CNN	92.23	93	95.18	91.7	89.2	92
Mobile Net	89.5	69.9	95.6	88.2	95	93.3
Google Net	94	89.6	88.2	78.9	95.4	97.30
InceptionV3	90.2	92.4	88.4	92.5	59.67	69.32
Ensemble classifier	95.46	96.11	87.7	92.9	96.27	92.21
Custom CNN	92.4	93.2	90	92.5	88.7	88.12
U Net	94.78	86.49	90.4	86.3	88.24	89.37
Proposed	98.8	98.28	98	97.5	98.85	97.8

#### 4. Conclusion

Long-term diabetes is the cause of the degenerative eye condition known as diabetic retinopathy. If not detected in its early stages, it may cause blindness. This paper proposes an automated approach for DR categorization of PDR, moderate DR, severe DR, mild DR, and no DR called EfficientNet-B0, which is based on the Modified Sparrow Search Algorithm (EMSSA). The proposed method uses a modified version of histogram equalization to preprocess DR pictures. The segmentation methodology's findings show that, in terms of outcomes, the sparse subspace clustering technique performs better than other contemporary methods that have been discussed in the literature. The next step in the plan was to apply a dimensionality reduction approach to the segmented region to streamline the classification process. At long last, the prescribed EMSSA is applied to characterize the images into five phases. PDR, no DR, mild DR, severe DR, and moderate DR. The proposed arrangement EMSSA decreases the complexity of the framework by utilizing reduced dimensional information. Various information and image expansion strategies are attempted, trying to upgrade the presentation of the proposed model. The proposed classification model accomplishes improved results: 99.8% characterization accuracy, 98.2% recall value, 98% specificity, 98.85% precision value, and 97.8% F-score. Ultimately, it is verified that, in comparison to the current models, the suggested EMSSA performs better at identifying DR. Future research should focus on implementing the EMSSA-based DR classification model in real-world clinical settings by integrating it with automated screening systems and mobile applications for remote diagnosis. Furthermore, verifying the model on varied populations, assuring regulatory compliance, and integrating it with electronic health records might help it become more feasible and widely adopted in healthcare.

**Author contributions:** Study conception and design, MVM and AKC; data collection, MVM and AKC; analysis and interpretation of results, MVM and AKC; draft manuscript preparation: MVM and AKC. All authors have read and agreed to the published version of the manuscript.

**Availability of data and material:** The data that support the findings of this study are available from the corresponding author, upon reasonable request.

**Informed consent:** I certify that I have explained the nature and purpose of this study to the above-named individual, and I have discussed the potential benefits of this study participation. The questions the individual had about this study have been answered, and we will always be available to address future questions.

**Conflict of interest:** The authors declare no conflict of interest.

## References

1. Modi P, Kumar Y. Smart detection and diagnosis of diabetic retinopathy using bat based feature selection algorithm and deep forest technique. *Computers & Industrial Engineering*. 2023; 182: 109364. doi: 10.1016/j.cie.2023.109364
2. Parthiban K, Kamarasan M. Diabetic retinopathy detection and grading of retinal fundus images using coyote optimization algorithm with deep learning. *Multimedia Tools and Applications*. 2022; 82(12): 18947-18966. doi: 10.1007/s11042-022-14234-8
3. Nunez dR, Joan M, Paul N, et al. Using deep learning to detect diabetic retinopathy on handheld non-mydratric retinal images acquired by field workers in community settings. *Scientific reports*; 2023.
4. Bhimavarapu U, Chintalapudi N, Battineni G. Automatic Detection and Classification of Diabetic Retinopathy Using the Improved Pooling Function in the Convolution Neural Network. *Diagnostics*. 2023; 13(15): 2606. doi: 10.3390/diagnostics13152606
5. Raiaan MAK, Fatema K, Khan IU, et al. A Lightweight Robust Deep Learning Model Gained High Accuracy in Classifying a Wide Range of Diabetic Retinopathy Images. *IEEE Access*. 2023; 11: 42361-42388. doi: 10.1109/access.2023.3272228
6. Surya J, Neha P, Tyler HR, et al. Efficacy of deep learning-based artificial intelligence models in screening and referring patients with diabetic retinopathy and glaucoma. *Indian Journal of Ophthalmology*. 2023.
7. Pradeep J, Erick Jeffery N, Saranraj M, Nasser Hussain J. Enhanced Recognition system for Diabetic Retinopathy using Machine Learning with Deep Learning Approach. *Journal of Population Therapeutics and Clinical Pharmacology*. 2023; 30(11): 452-466. doi: 10.47750/jptcp.2023.30.11.047
8. Dungrani DR, Rajesh Lotia H, Parikh DV, et al. Detection and Classification of Diabetic Retinopathy using Deep Learning. *Proceedings of the 2023 5th Biennial International Conference on Nascent Technologies in Engineering (ICNTE)*; 2023. doi: 10.1109/icnte56631.2023.10146626
9. Sinha BB, Dhanalakshmi R, Balakrishnan K. Early diagnosis of diabetic retinopathy using deep learning techniques. *Computational Methods and Deep Learning for Ophthalmology*; 2023. doi: 10.1016/b978-0-323-95415-0.00006-1
10. Sangamesh H, Vishwanath Petli VK, Jalihal BK, et al. A New Approach to Recognize a Patient with Diabetic Retinopathy using Pre-trained Deep Neural Network EfficientNetB0. *Proceedings of the 2023 IEEE International Conference on Integrated Circuits and Communication Systems (ICICACS)*; 2023. doi: 10.1109/icicacs57338.2023.10099647
11. Gorde KS, Gurjar AA. A Comparative Analysis on Diabetic Retinopathy using Deep Learning and Nature based Optimization Algorithms. *Proceedings of the 2023 International Conference on Intelligent Systems, Advanced Computing and Communication (ISACC)*; 2023. doi: 10.1109/isacc56298.2023.10083804
12. Srinivasan S, Nagarnaidu Rajaperumal R, Mathivanan SK, et al. Detection and Grade Classification of Diabetic Retinopathy and Adult Vitelliform Macular Dystrophy Based on Ophthalmoscopy Images. *Electronics*. 2023; 12(4): 862. doi: 10.3390/electronics12040862
13. Singla C, Ravneet K, Janpreet S, et al. Fine Tuned Pre-Trained Deep Neural Network for Automatic Detection of Diabetic Retinopathy Using Fundus Images. *International Journal of Intelligent Systems and Applications in Engineering*. 2023.

14. Basheer S, Varghese RE. Estimation of diabetic retinopathy using deep learning. *Proceedings of the international conference on research advances in engineering and technology—ITechcet* 2022; 2024. doi: 10.1063/5.0194492
15. Murugan A, Ashok B, Dhanush M, Elankathir S. Automatic Classification and Earlier Detection of Diabetic Retinopathy Using Deep Learning. *Proceedings of the 2023 9th International Conference on Advanced Computing and Communication Systems (ICACCS)*. 2023. doi: 10.1109/icaccs57279.2023.10113025
16. Dinpajhouh M, Seyyedsalehi SA. Automated detecting and severity grading of diabetic retinopathy using transfer learning and attention mechanism. *Neural Computing and Applications*. 2023; 35(33): 23959-23971. doi: 10.1007/s00521-023-09001-1
17. Saxena S, Kumar A, Goel A. Detection of diabetic retinopathy using deep learning. *Artificial Intelligence, Blockchain, Computing and Security*; 2023: 65-70. doi: 10.1201/9781032684994-11
18. Ashwini K, Dash R. Grading diabetic retinopathy using multiresolution based CNN. *Biomedical Signal Processing and Control*. 2023; 86: 105210. doi: 10.1016/j.bspc.2023.105210
19. Özbay E. An active deep learning method for diabetic retinopathy detection in segmented fundus images using artificial bee colony algorithm. *Artificial Intelligence Review*. 2022; 56(4): 3291-3318. doi: 10.1007/s10462-022-10231-3
20. Maaliw RR, Mabunga ZP, De Veluz MRD, et al. An Enhanced Segmentation and Deep Learning Architecture for Early Diabetic Retinopathy Detection. *Proceedings of the 2023 IEEE 13th Annual Computing and Communication Workshop and Conference (CCWC)*; 2023. doi: 10.1109/ccwc57344.2023.10099069
21. Sebastian A, Elharrouss O, Al-Maadeed S, et al. A Survey on Deep-Learning-Based Diabetic Retinopathy Classification. *Diagnostics*. 2023; 13(3): 345. doi: 10.3390/diagnostics13030345
22. Uppamma P, Bhattacharya S. Deep Learning and Medical Image Processing Techniques for Diabetic Retinopathy: A Survey of Applications, Challenges, and Future Trends. *Journal of Healthcare Engineering*. 2023; 2023(1). doi: 10.1155/2023/2728719
23. Mohanty C, Mahapatra S, Acharya B, et al. Using Deep Learning Architectures for Detection and Classification of Diabetic Retinopathy. *Sensors*. 2023; 23(12): 5726. doi: 10.3390/s23125726
24. Fayyaz AM, Sharif MI, Azam S, et al. Analysis of Diabetic Retinopathy (DR) Based on the Deep Learning. *Information*. 2023; 14(1): 30. doi: 10.3390/info14010030
25. Venkaiahppalawamy B, Prasad Reddy P, Batha S. Hybrid deep learning approaches for the detection of diabetic retinopathy using optimized wavelet based model. *Biomedical Signal Processing and Control*. 2023; 79: 104146. doi: 10.1016/j.bspc.2022.104146
26. Gao Z, Pan X, Shao J, et al. Automatic interpretation and clinical evaluation for fundus fluorescein angiography images of diabetic retinopathy patients by deep learning. *British Journal of Ophthalmology*. 2022; 107(12): 1852-1858. doi: 10.1136/bjo-2022-321472
27. Agarwal S, Bhat A. A survey on recent developments in diabetic retinopathy detection through integration of deep learning. *Multimedia Tools and Applications*. 2022; 82(11): 17321-17351. doi: 10.1007/s11042-022-13837-5
28. Hemanth SV, Alagarsamy S. Hybrid adaptive deep learning classifier for early detection of diabetic retinopathy using optimal feature extraction and classification. *Journal of Diabetes & Metabolic Disorders*. 2023; 22(1): 881-895. doi: 10.1007/s40200-023-01220-6